Identifying the optimal phenological period for discriminating subtropical fruit tree crops using multi-temporal Sentinel-2 data and Google Earth Engine

Yingisani Chabalala [1,2]*, Elhadi Adam [2] and Khalid Adem Ali [2,3]
[1]University of Witwatersrand, Faculty of Science, School of Geography, Archaeology and Environmental Studies, Johannesburg, 2000
[2]University of South Africa, Science Campus, Department of Environmental Science, Johannesburg, 1710
[3]Department of Geology and Environmental Geosciences, College of Charleston, 29424, SC, USA
* Correspondence: ywchabalala@gmail.com; Tel.: +27725899389

DOI: http://dx.doi.org/10.4314/sajg.v12i.2.10

Abstract

The accurate and appropriate monitoring of the spatial distribution of fruit tree crops is crucial for crop management and yield forecasting. Owing to both inter- and intra-farm fragmentation and overlapping phenological cycles, the classification of fruit tree crops in subtropical agriculture using single-date images is challenging. Therefore, this research aimed to identify the optimal temporal window in which the crucial phenological stages can be used to classify fruit tree crops in Levubu, Limpopo province, using a random forest (RF) classifier. Phenological metrics were extracted from 12-month Multispectral Instrument (MSI) images from Sentinel-2 (S2). The RF classification algorithm attained an overall accuracy of 84.89% and a kappa coefficient of 83%. The user accuracy ranged from 62 to 100%, while the producer accuracy ranged from 60 to 100%. An analysis of variance was used to assess whether the overall accuracies among the S2 monthly composites were statistically significant. The results showed distinct spectral differences between fruit trees. In April, there were differences observed during the harvesting and senescence of the mango and macadamia nut crops. In May, there were differences observed during the senescence of the macadamia nut, mango, and guava crops. In June and July, there were distinct spectral differences during the peak flowering stage of the avocado, macadamia nut, and mango crops, as well as in the fruiting stage of the banana crops. Followed by the red-edge bands, the shortwave infrared bands were significant in differentiating between the respective fruit tree crops. The results of this research provide evidence-based information that can assist farm managers and horticulturists in making informed decisions. This is critical in achieving effective agricultural management and in ensuring the sustainability of local horticultural systems.

Keywords: *fruit trees, crop mapping, Sentinel-2, random forest, Google Earth Engine*

1. Introduction

Mapping crop types is an important activity that provides evidence-based information for guiding agricultural practices and policies for food security (Jin *et al.*, 2019). Accurate and timely maps showing the spatial distribution of crop types provide valuable information for monitoring crops, estimating yields, scheduling agronomic practices, and detecting crop anomalies (Remelgado *et al.*, 2020). Moreover, crop type maps can determine the ecological suitability for extending the existing crop production area and for increasing the volume of harvested products (Singh *et al.*, 2017). Crop type mapping using remote sensing is an efficient method for assessing agricultural production. Satellite sensors such as the Sentinel-2 (S2) Multispectral Imager (MSI) and the Landsat 8 Operational Land Imager (OLI) have medium and high spatial and temporal resolutions that provide information suitable for crop modelling (Neigh *et al.*, 2018). Owing to the spectral similarity among specific tree species during their phenological stage, the mapping of crop types using single-date images may not be sufficient (Mercier *et al.*, 2020). Fruit tree species are the only crop types that have a stable canopy cover and a similar leaf structure (Asgarian *et al*., 2016). This results in overlapping spectral signatures which impair accuracy in the classification process (Neigh *et al.*, 2018; Nabil *et al.*, 2022). For example, Chabalala *et al*. (2022) applied a random forest (RF) classifier to a S2 single-date image and reported misclassifications of mango and avocado crops which were attributed to overlapping spectral reflectance. Therefore, multi-temporal data based on key crop growth and phenology stages can serve as a promising approach to spectrally distinguishing between tree species and improve the accuracy in classifying tree species (Peña-Barragán *et al*., 2011).

Several studies have used multi-temporal remote sensing information and different classifiers to predict vegetation greenness across key crop growth stages in various agricultural landscapes (Luo *et al.*, 2021; Shelestov *et al.*, 2017). Nabil *et al*. (2022) applied a RF classifier to S2 time series data to map fruit tree crops in Egypt and obtained an overall classification accuracy of 96%, while Busetto *et al*. (2019) analysed temporal changes in rice crops in Senegal (West Africa) using Moderate Resolution Imaging Spectroradiometer (MODIS) time series data and the PhenoRice algorithm. The latter researchers obtained an overall accuracy of 81% and 65% for dry and wet seasons, respectively. Pena *et al*. (2017) used Landsat-8 time Evaluation of Sentinel-1 and Sentinel- 2 time series for predicting wheat and rapeseed phenological stages series data to classify fruit tree crops in Chile, and accurate results were achieved using linear discriminant analysis during the crop green-up stage. Zurita-Milla *et al.* (2017) obtained an overall accuracy of 80% when identifying crop types in smallholder agriculture in sub-Saharan Africa using Worldview-2 time series data and a RF classifier. Similarly, Zhang *et al.* (2018) improved crop-type classification accuracy in Ontario, Canada, using a RF classifier and Satellite pour l'Observation de la Terre (SPOT-5) time-series data. However, most of these studies were conducted at regional and country levels (Kumari *et al*., 2021; Wang, Zhai and Zhang, 2021; Kraaijvanger *et al.*, 2019). Because of the challenges regarding the suitability and consistency of these mapping approaches, they cannot be easily replicated in different contexts, such as in the highly fragmented African agricultural environments (You and Dong, 2020).

Farming systems have site-specific characteristics that influence the spatial and spectral information of crops—this determines how different crop types can be accurately distinguished from one another. Studies

such as Luo *et al.* (2021), Shelestov *et al. (*2017), and You and Dong (2020) used remote sensing data at Google Earth Engine (GEE) to map crop types. However, these studies were conducted in areas such as China and Ukraine, which have site-specific characteristics that differ from those of the Levubu subtropical farms. Subtropical agriculture in Levubu is characterised by highly fragmented farms growing clonal fruit trees, with minimal seasonal growth dynamics associated with overlapping phenological cycles (Neigh *et al.*, 2018). The mapping of fruit trees in smallholder agriculture is complex, owing to agronomic factors such as wide-ranging cropping patterns, numerous crop varieties, different crop-growth calendars, and high crop densities (Nabil *et al.*, 2022; Wang *et al*., 2021). Smallholder agriculture is characterised by diverse and patchy fragmented landscapes, a variety of management practices, and varying agro-climatic conditions (Potgieter *et al.*, 2021). The spectral behaviour of fruit tree crops in such landscapes presents challenges in crop observation when optical sensors with coarse or medium spatial resolutions are used.These images may not correspond with the ideal period optimal for inter-class separation (Pena *et al*., 2017; Shelestov *et al.*, 2017; Lamour *et al.*, 2019).

Identifying optimal growth periods and the phenological traits of fruit-tree crops using high temporal resolution remote sensing data can be applied to develop a robust method for identifying fruit-tree species (Mercier *et al.*, 2020). Copernicus (European Space Agency) offers optical constellation missions, such as S2, with high spatial and temporal resolutions suitable for accurately identifying crop types (Lamour *et al.*, 2019; Gao *et al*., 2020). The mission provides opportunities for smallholder farmers to adopt sustainable farming technologies by accelerating smart and effective crop mapping (Shelestov *et al*., 2017). Furthermore, it facilitates the development of operational mapping tools that will encourage the continued use of earth observation data in monitoring crop types in smallholder landscapes in Africa at the local, regional, and national levels (Arias *et al*., 2020; Veloso *et al.*, 2017). However, the effective use of S2 timeseries data for the detection of crop types is still limited, especially in smallholder subtropical agriculture (Veloso *et al.*, 2017).

The objective of this research was to identify the optimal phenological window in which fruit trees can be effectively classified in a highly heterogeneous horticultural landscape in Levubu, Limpopo province, South Africa, using phenological metrics derived from multi-temporal S2 data and a RF classifier. This method provided evidence-based information that would enable efficient horticultural monitoring systems and sustainable agricultural management (Usha and Singh, 2013).

2. Materials and Methods

2.1. Research area

Levubu is in Limpopo Province, northeastern South Africa (Figure 1) and the fruit-farming area covers *c.* 10,000 hectares (Fraser, 2008). The elevation varies from 677 to 2221 m, with extensive flat and fertile areas in the plains to the southeast of the Makhado local municipal area. The sub tropical climate has temperatures ranging from 16 to 40°C during summer (i.e., from December to February), and 12 to 22°C in winter (i.e., from May to August). The area has an average annual rainfall of 340 mm. The research area has diverse agricultural landscapes and agro-meteorological conditions that influence the performance and management

of fruit tree crops. The fruit trees commonly planted in the area are avocado, banana, guava, mango, and macadamia nut.

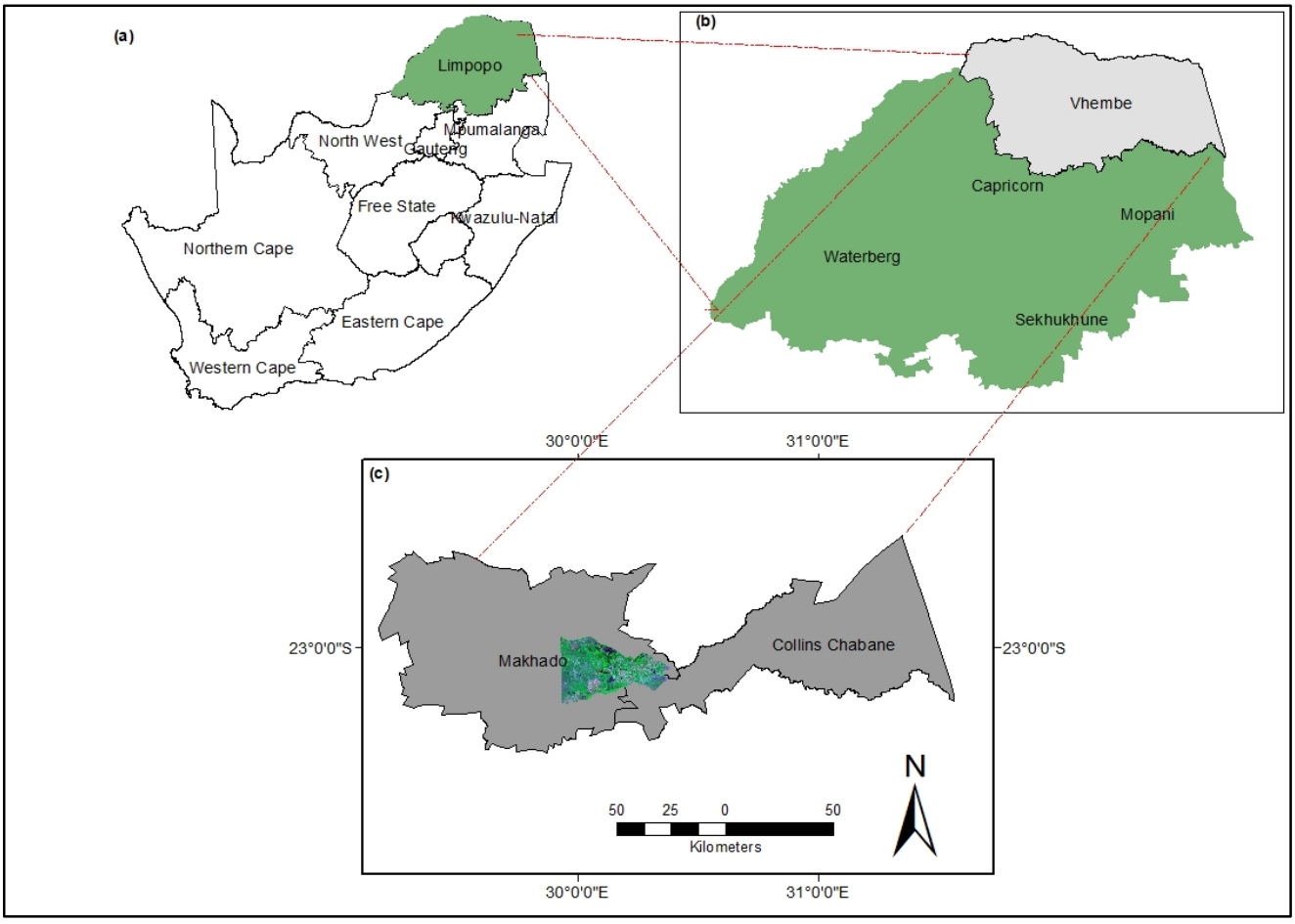

Figure 1: Geographic location of Levubu subtropical farming area in Makhado and Collins Chabane Local Municipalities, Limpopo Province, South Africa.

2.2. Earth observation data and pre-processing

2.2.1. Sentinel-2 data and pre-processing

This study used Copernicus/S2 SR ImageCollection, and all available data from June 2019 to May 2020 were sourced. The Copernicus/S2 SR is a Level-2A Surface Reflectance ImageCollection that is atmospherically corrected and made freely available for public consumption on GEE (https://developers.google.com/earth-engine/datasets/catalog/COPERNICUS_S2_SR) (European Space Agency, 2023). The ImageCollection has 11 bands, namely, four visible bands (B1, B2, B3, B4)), three red-edge bands (B5, B6, B7), two near-infrared bands (B8, B8A), and two shortwave bands (B11, B12) (European Space Agency, 2023). Integrating spectral bands and vegetation indices allows for a means to determine redundancy and correlation, which in turn affects the classification accuracy (Peña-barragán *et al*., 2011). Hence, the research used only the spectral data acquired at 10 and 20m (i.e., blue (B2), green (B3), red (B4), red-edge (B5, B6, B7, and B8A), near-infrared (B8), and shortwave-infrared (B11 and B12) bands). Fewer

images were available for the summer months owing to the dense cloud cover during that season. Table 1 shows the spatial and spectral properties of the Sentinel-2 (S2) data. The optimal temporal window for accurate tree crop and co-existing land cover mapping was identified using a median composite method, which synthesises the pixels of the available timeseries images(Luo *et al*., 2021). Owing to the variation in cloud cover, the monthly composites included different numbers of images for each month . They were created using all images acquired with a maximum filter of five percent (5%) cloud cover each month.

Table 1: Spectral configurations for the S2 ImageCollection used from GEE.

S2 MSI				
Band	Description	Pixel Size (m)	Wavelength Centre	Wavelength Width
B1	Coastal aerosol	60	443	20
B2	Blue	10	490	65
B3	Green	10	560	35
B4	Red	10	665	30
B5	Red-edge 1	20	705	15
B6	Red-edge 2	20	740	15
B7	Red-edge 3	20	783	20
B8	Near-infrared (NIR)	10	842	115
B8A	Red-edge 4 (NIR narrow)	20	865	20
B9	Water vapour	60	945	20
B11	SWIR	20	1375	30
B12	SWIR	20	2190	180
QA60	Cloud mask	60		

The ImageCollection used in this study to map the fruit tree crops and the surrounding land cover types was S2 SR. It was applied to the data acquired for the agronomic year, June 2019 - May 2020 (i.e., 12 months). A total of 18 S2 images (Table 2) were collected monthly, equating to 216 images for the study period. As commonly observed in sub tropical regions, the monthly composites were affected by clouds and shadow clouds. The S2 cloud masking was computed using the QA60 band that combines the cirrus cloud and dense cloud masks (Jin *et al*., 2019). The QA60 band has a spatial resolution of 60m and is provided with S2 SR data in the GEE platform (Claverie *et al*., 2018; Kolecka *et al*., 2018).

Table 2: Number of Sentinel-2 images acquired for each monthly period for the Levubu sub tropical farm region.

S2 monthly composites	
Month	Number of images
January	18
February	18
March	18
April	18
May	18
June	18
July	18
August	18
September	18
October	18
November	18
December	18

2.3. Acquisition of ground control points

Coinciding with the acquisition of image data for the respective crop growing seasons (Table 2), the field survey to map common fruit trees and other land cover types was conducted in December 2019, January, and April 2020. A Global Positioning System (eTrex® 20x GPS Receiver; Garmin, Olathe, KS, USA), with a positional accuracy of five metres (5 m) was used to record the longitudinal and latitudinal locations of the fruit-tree crops common in the area. A total number of 304 (n=304) ground-truth points were mapped for the dominant land-cover classes, including avocado (n=49), banana (n=53), built-up area (n=7), guava (n=12), macadamia nut (n=95), mango (n=18), pine tree (n=22), water body (n=4) and woody vegetation (n=44). The collected (n = 304) GPS points were used to guide the digitilisation of additional points in cases where field sizes were big enough; this was achieved by using informative observations on Google Earth Pro and ArcGIS (Chabalala *et al*., 2022).

Field surveys conducted in smallholder areas are challenging, and some of the collected data were imbalanced owing to fragmented landscapes and the lack of access to some parts of the study area (Ren *et al.*, 2022). Because the unproportional distribution of the field data could affect classification accuracy (Maxwell et al., 2018), field-mapped points (n=304) were used to guide the digitalisation of additional points in the data-scarce regions to account for this bias (Ni *et al.*, 2021). This approach resulted in 1894 points, which were then split into training and validation sets by using the ratio, 70:30. This approach has proved to be robust in mapping fruit trees with varied phenological growth characteristics (You and Dong, 2020). The growth stages of fruit tree crops across the Levubu subtropical farming region are presented in Table 3.

Table 3: Growth stages of fruit trees in the Levubu subtropical farming area (Note: The shades denote the flowering stage (Flo), fruiting stage (Fru), and harvesting stage (Harv).

Class	Varieties	Jan	Feb	Mar	Apr	May	June	July	Aug	Sept	Oct	Nov	Dec
Avocado	Hass	Fru	Fru	Fru	Fru	Harv	Harv			Flo	Flo	Flo	Fru
	Fuerte	Fru	Harv	Harv						Flo	Flo	Flo	Fru
	Pinkerton	Fru	Fru	Fru	Harv	Harv			Flo	Flo	Flo	Fru	Fru
	Ryan	Flo	Flo	Fru	Fru	Fru	Fru	Harv	Harv				Flo
Banana		Harv	Harv	Flo	Flo	Flo	Fru	Fru	Fru	Fru	Harv	Harv	Harv
Guava		Fru	Fru	Fru	Harv							Flo	Flo
Macadamia nut	Beaumont 695	Fru	Fru	Fru	Harv	Harv			Flo	Flo	Fru	Fru	Fru
	Nelmak 2	Fru	Harv	Harv			Flo	Flo	Fru	Fru	Fru	Fru	Fru
	A4	Fru	Harv	Harv			Flo	Flo	Fru	Fru	Fru	Fru	Fru
	814	Fru	Harv	Harv			Flo	Flo	Fru	Fru	Fru	Fru	Fru
	816	Fru	Harv	Harv			Flo	Flo	Fru	Fru	Fru	Fru	Fru
	344	Fru	Harv	Harv			Flo	Flo	Fru	Fru	Fru	Fru	Fru
Mango	Tommy Atkins	Harv						Flo	Flo	Fru	Fru	Fru	Harv
	Sabre						Flo	Flo	Fru	Fru	Fru	Harv	Harv
	Keitt	Fru	Harv	Harv						Flo	Flo	Fru	Fru

2.4. Feature extraction

Optimal selection of remote sensing data is crucial for the efficient mapping of crop types. In this research, the optimal phenological window was identified by developing 12 monthly composite-based models (i.e., January to December). In a Google Earth Engine (GEE) environment, the collected ground-truth points (GCPs) were overlaid on the monthly composites and used to extract the multi-temporal phenological metrics (i.e., Flo (flowering), Fru (fruiting), and Harv (harvesting) used to train and classify the fruit trees.

2.5. Spectral separability of fruit tree crops

The first step in the classification of tree species is to determine whether the classes are spectrally different. For this research, the spectral information was extracted from the Sentinel-2 images using the point data collected from the field. The assessment of the spectral properties of the sample training classes and their separability over others was conducted using spectral reflectance curves.

2.6. Training of the random forest classifier

The random forest (RF) classifier is an ensemble tree-based classifier developed in 2001 (Breiman, 2001). It combines random sub-control methods and integrated learning theory, making it suitable for processing heterogeneous data with high dimensionality (Zhi *et al.*, 2022). The random forest (RF) classifier has been extensively used because of its high accuracy, robustness, feature importance, and scalability (Tatsumi *et al.*, 2015; Saini and Ghosh, 2018; Chabalala *et al.*, 2023). Also, the RF classifier is less sensitive to noise and correlations that are intrinsically inherited in remote sensing data and reduces overfitting by averaging multiple decision trees. As such, it is suitable for mapping crop types in heterogeneous landscapes (Tatsumi *et al.*, 2015; Saini and Ghosh, 2018; Chabalala *et al.* 2023). Two parameters were adjusted when training the

RF model in the GEE environment: 1) the *ntree,* which was set to a default value of 500. It determines the total number of binary trees that can be used to build a RF model. An increase in the number of trees results in an increase in the cost calculation; 2) the *mtry* parameter was set as a square root of the total number of the input variables (Kraaijvanger *et al.*, 2019). About 67% of the samples from the training dataset were regarded as in-bag, while the remaining one-third (i.e., 33%) were termed out-of-bag (OOB) samples (Kraaijvanger *et al.*, 2019). The performance of the RF classification was examined and optimised using a 10-fold cross-validation (Tatsumi *et al*., 2015).

2.7. Accuracy assessment

Accuracy assessment is crucial when analysing remote sensing data (Banko, 2016). An accuracy assessment tests the effectiveness of the applied methodology in predicting the data (Olofsson *et al.*, 2014). For this study, the accuracy of the classified images was assessed using 30% (validation data) of the reference data. A confusion matrix was used to calculate the three metrics (i.e., the overall classification accuracy (OA), the user accuracy (UA), the producer accuracy (PA), and the kappa coefficients (κ), all of which were used to interpret the results of the models (Congalton, 1991; Olofsson *et al.*, 2014).

2.8. Statistical analysis to determine the reliability of the research results

The reliability of the research results was tested by comparing results from a one-way analysis of variance (ANOVA) and the student's paired t-test, conducted at a 0.5% confidence level (Gutierrez-Coarite *et al*., 2018; Bagheri, 2019).

3. Results

3.1. Spectral separability between fruit tree crops

The mean spectral reflectance curves of the training data were extracted from the S2 data for the respective months and plotted with their standard deviations (Figure 3). Generally, all fruit tree classes exhibited considerable spectral overlaps. In April, only the green band (B3) separated macadamia from the other four classes beyond one standard deviation of uncertainty. In May, the green band (B3) differentiated avocado trees from the other classes, while the shortwave-infrared (B11 and B12) bands separated guava from the remaining four classes beyond one standard deviation of uncertainty. In the months of June and July, the shortwave-infrared (B11 and B12) bands again differentiated guava from the avocado, banana, macadamia nut, and mango trees from the remaining four classes. The lowest spectral reflectance values were recorded by the green band (B3) for macadamia nut in April and avocado in May.

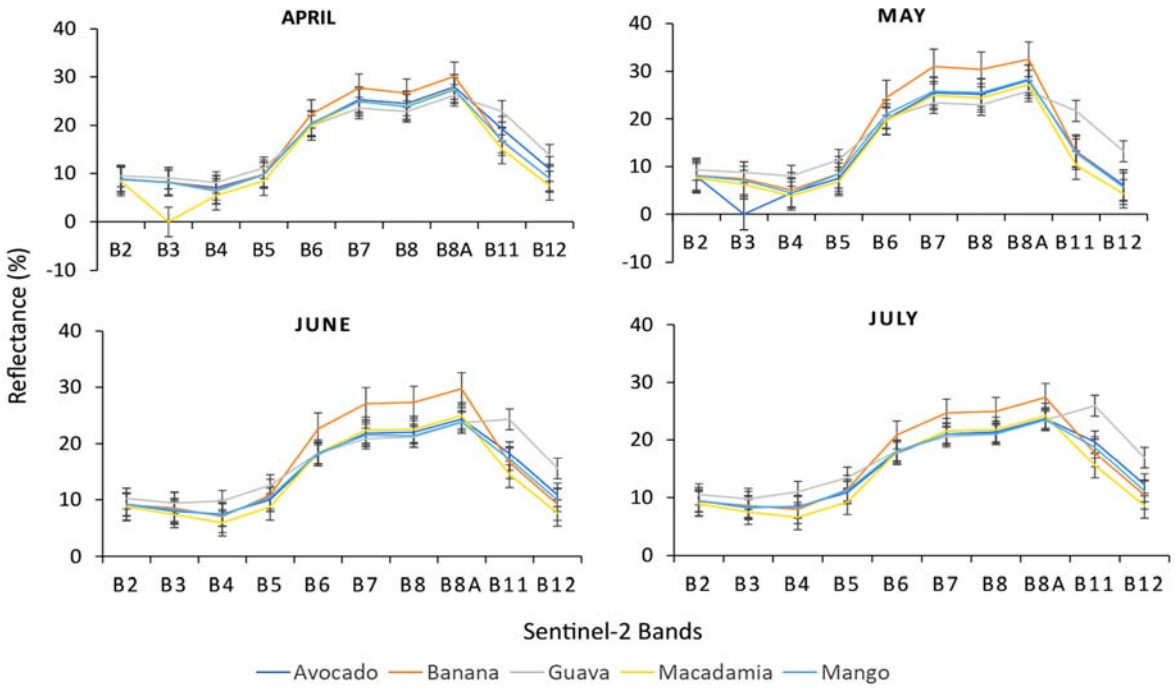

Figure 3: Spectral signatures of fruit tree crops at various growth stages extracted from Sentinel-2 images in 2019 (June and July) and 2020 (April and May): blue (B2), green (B3), red (B4), red-edge (B5, B6, B7, and B8A), near-infrared (B8), and shortwave-infrared (B11 and B12) bands.

3.2. Relative importance of variables

The Sentinel-2 (S2) data acquired in April to July—during the peak of crop productivity—were crucial in differentiating between fruit trees in Levubu. Figure 4 shows the performance of predictors applied in modelling fruit-tree crops using the variable importance tool in the random forest (RF) classifier for the winter months (i.e., April-July — the months that produced the highest overall accuracy (OA)). The red band (B4: 665 nm) ranked the highest for the months of May - July, followed by the green band in April. During the peak of the flowering (August-December) and fruiting (January - March) stages, the fruit trees differed distinctly from the surrounding land use/land cover (LULC) types, i.e., built-up area, pine tree, other woody vegetation, bare soil, and water body. The blue band (B2: 490 nm) was a strong predictor in May, followed by the shortwave-infrared band (B11:1610 nm) in May and June. The shortwave-infrared band (B11:1610 nm) was a strong predictor in April, while the shortwave-infrared (B11: 1610 nm) and the red-edge (B5:705 nm) bands were strong in April, May, June, and July. Overall, the results show-case the importance of the visible bands (i.e., B2:490 nm, B3:560 nm, and B4:665 nm), the shortwave-infrared bands (i.e., B11:1610 nm and B12:2190 nm), and the red-edge bands (i.e., B5:705 nm and B7:740 nm) in differentiating between the fruit tree crops.

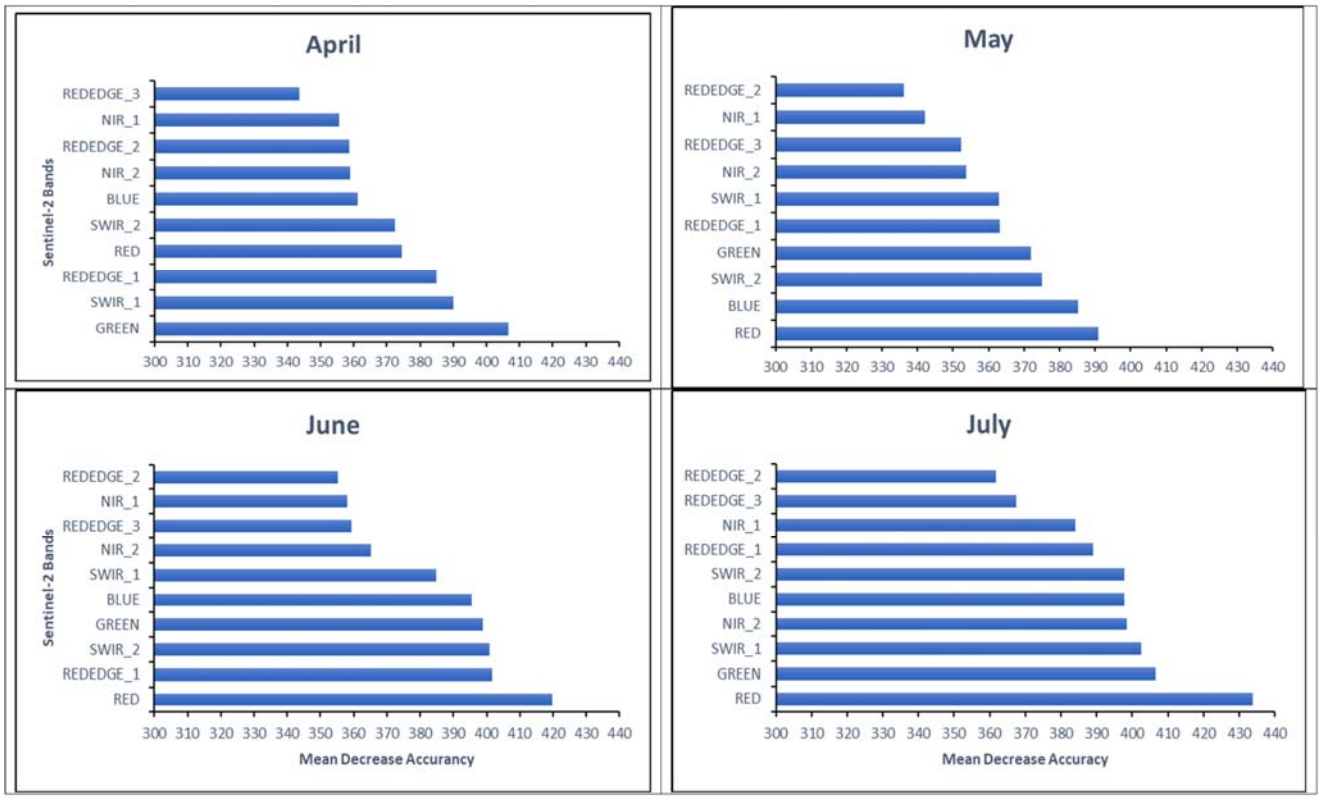

Figure 4: Variable importance of bands in the best performing models used in mapping fruit trees using the Sentinel-2 dataset: (a) April, (b) May, (c) June, and (d) July.

3.3. Accuracy assessment

The highest classification accuracy was obtained for the winter Sentinel-2 (S2) images (i.e., April (81.16%), May (83.57%), June (81.87%), and July (84.89%)). The lowest classification accuracy was recorded for summer and autumn (i.e., August to March, with overall accuracies (OA) ranging from 70.07 to 78.82% and the kappa coefficient ranged from 67 to 83%. The OA and kappa coefficients (κ) for the 12-month S2 composites are presented in Figure 5.

Figure 6 presents the overall classifications and the accuracy statistics. The results show that the major land cover types are distinct from the fruit trees, with user accuracies (UA) of 70 - 100%. The differentiation between the fruit trees was fair in that the user (UA) and producer accuracies (PA) were between 60 and 100%. The most successful differentiation between the tree crops ability was achieved during the winter season (in order of merit in July, June, May, and April), while it was at its lowest level in August in the case of the avocado crop, where the UA and PA were 65% and 58.43%, respectively. The avocado crop recorded a similar UA of 69.93% and a PA of 70.86%, in October. In September, the banana crop recorded a UA and a PA of 62.5% and 74.53%, respectively. In January and February, the banana crop recorded a UA of 69.9% and a PA of 68.50%, while in March, the UA and PA declined to 62.90% and 68.42%, respectively. In January and February, the guava crop reported a UA of 65%. However, the PA was higher at 75%.

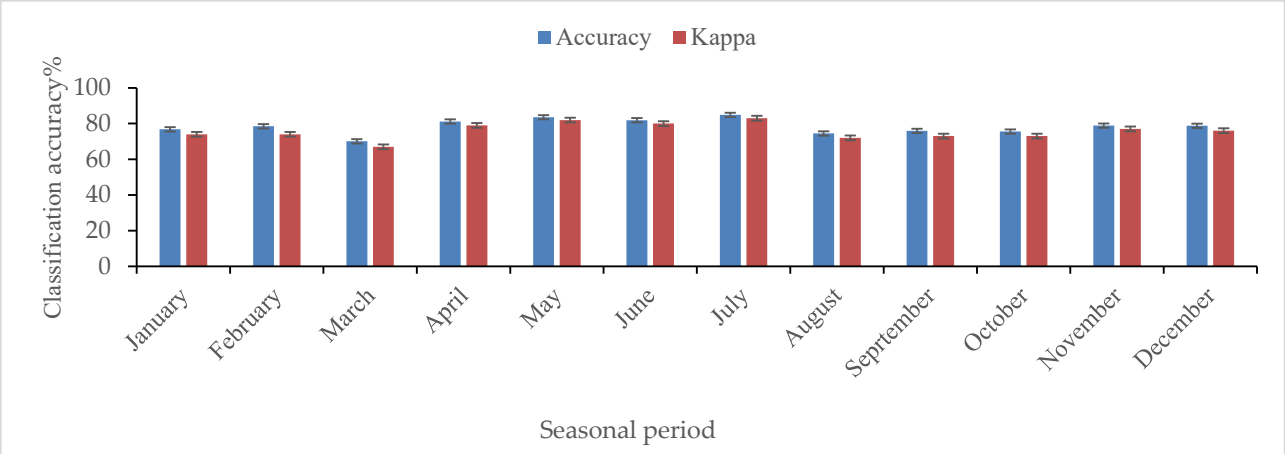

Figure 5: Comparison of the overall accuracy and kappa coefficients for the 12-month Sentinel-2 composites using a random forest classifier.

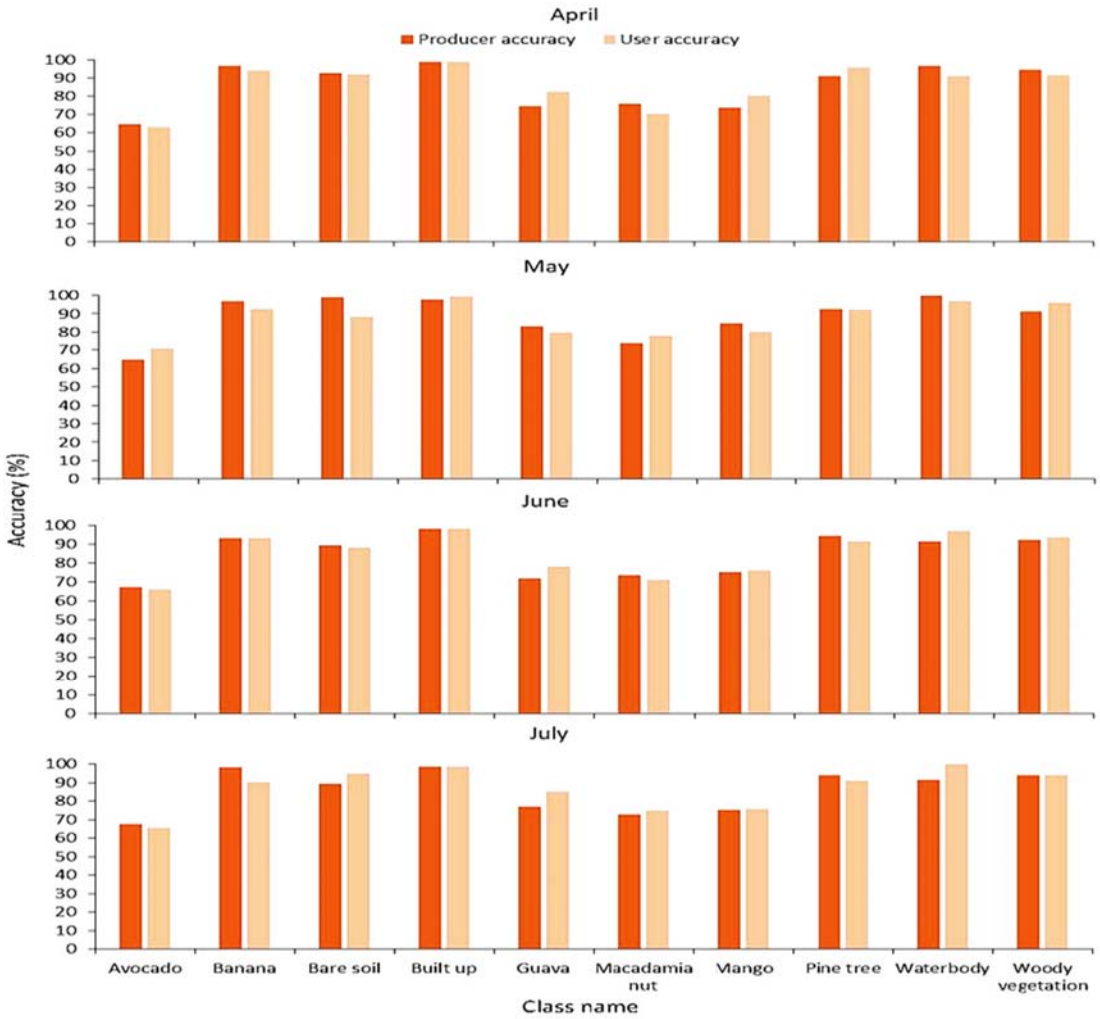

Figure 6: Producer and user accuracies for avocado, banana, bare soil, built-up, guava, macadamia nut, mango, pine tree, water body, and woody vegetation in Levubu, Limpopo Province, South Africa.

The predictions for mango for March, June, and August were low, with the UA ranging from 64 - 69% and the PA from 62 - 84%. The other land cover types (i.e., bare soil, built-up area, pine tree, other woody vegetation, and water body) had UAs of over 70% throughout the year, except for March, where a UA of 60.19% and a PA of 68.18% were obtained for the bare soil and pine tree classes, respectively.

3.4. Statistical analysis to determine the reliability of the research results

The changes in the RF accuracies were related to S2 monthly composites using ANOVA and the Student's t-test. The tests, conducted at a 95% confidence interval, produced a P-value of 0.170 and 0.174, greater than the confidence level of 0.05%, indicating an insignificant difference in the RF classifications across the twelve months.

3.5. Spatial distribution of fruit tree crops

Classified winter images show the predicted fruit tree crops and various land cover types within the study area (Figure 7). In the April image (Figure 7 and Figure 8A), the bare soil class covered 20.55 % of the study area, followed by the woody vegetation class with an areal coverage of 23.40%. In the same month, the avocado and macadamia nut classes covered approximately 11.15% and 16.01% of the study area, respectively. In May (Figure 7 and Figure 8B), woody vegetation was the dominant class, covering 22.20% of the study area. This was followed by the macadamia nut, avocado, built-up area, and banana classes, which recorded coverage of 10.90%, 16.60%, 7.05%, and 6.32%, respectively. Both guava and mango had more areal coverage than the avocado crop. In June (Figure 7 and Figure 8C), bare soil covered 30.29% of the study area and dominated the southeastern and southwestern parts of the research area, while woody vegetation covered 18.14%. Macadamia nut, built-up area, and avocado covered 11.01%, 11.83%, and 13.52%, respectively, of the area. All classes were separable in July (Figure 7 and Figure 8D) — where within-class misclassifications were low. The areal coverage of bare soil increased to 32.29% and continued to dominate in the southeastern and southwestern parts of the research area. The woody vegetation was concentrated in the southern and northern parts of the study area, covering 14.05% of the area. Avocado and macadamia nuts dominated the study area in the eastern, central, and north-western parts, covering 12.88% and 11.09%, respectively. Overall, the results demonstrate the potential of S2 multi-temporal data for mapping fruit trees in a highly fragmented heterogeneous horticultural landscape.

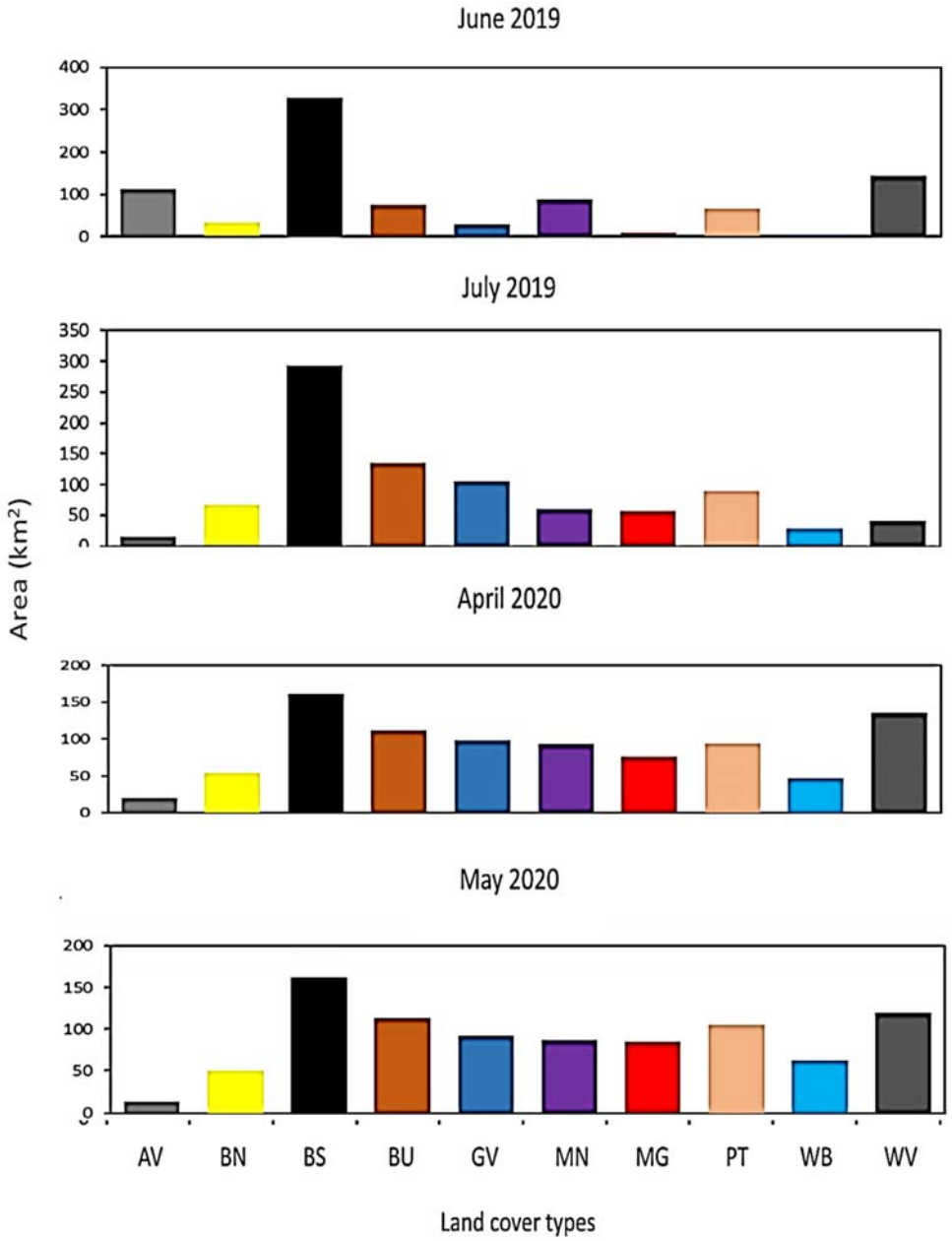

Figure 7. Areal coverage, in square kilometres, of fruit tree crops and co-existing land cover types in the study area. The areal calculations are based on the months of June 2019, July 2019, April 2020, and May 2020.

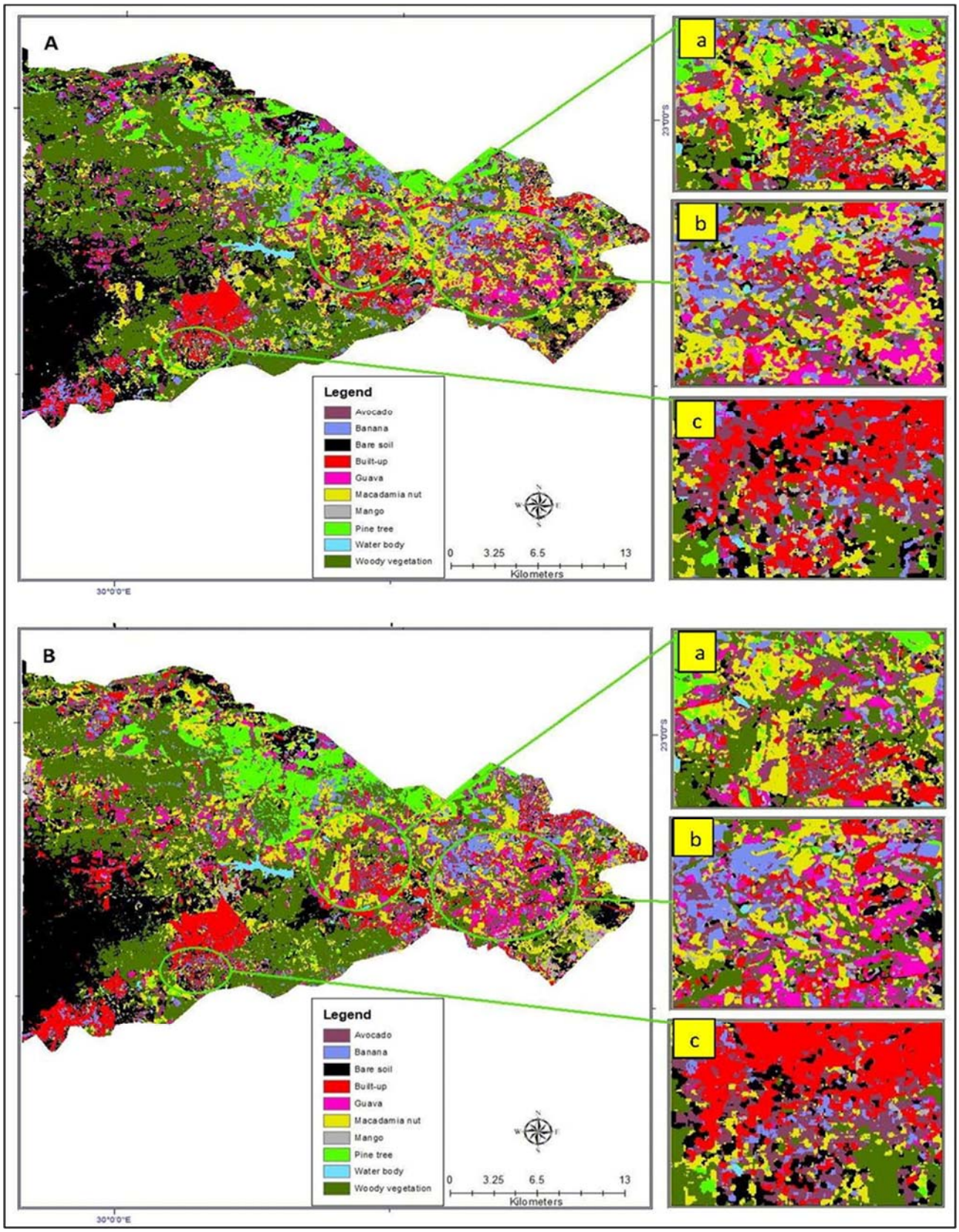
A
a
b
c
Legend
Avocado
Banana
Bare soil
Built-up
Guava
Macadamia nut
Mango
Pine tree
Water body
Woody vegetation
0 3.25 6.5 13
Kilometers
30°0'0"E
B
a
b
c
Legend
Avocado
Banana
Bare soil
Built-up
Guava
Macadamia nut
Mango
Pine tree
Water body
Woody vegetation
0 3.25 6.5 13
Kilometers
30°0'0"E

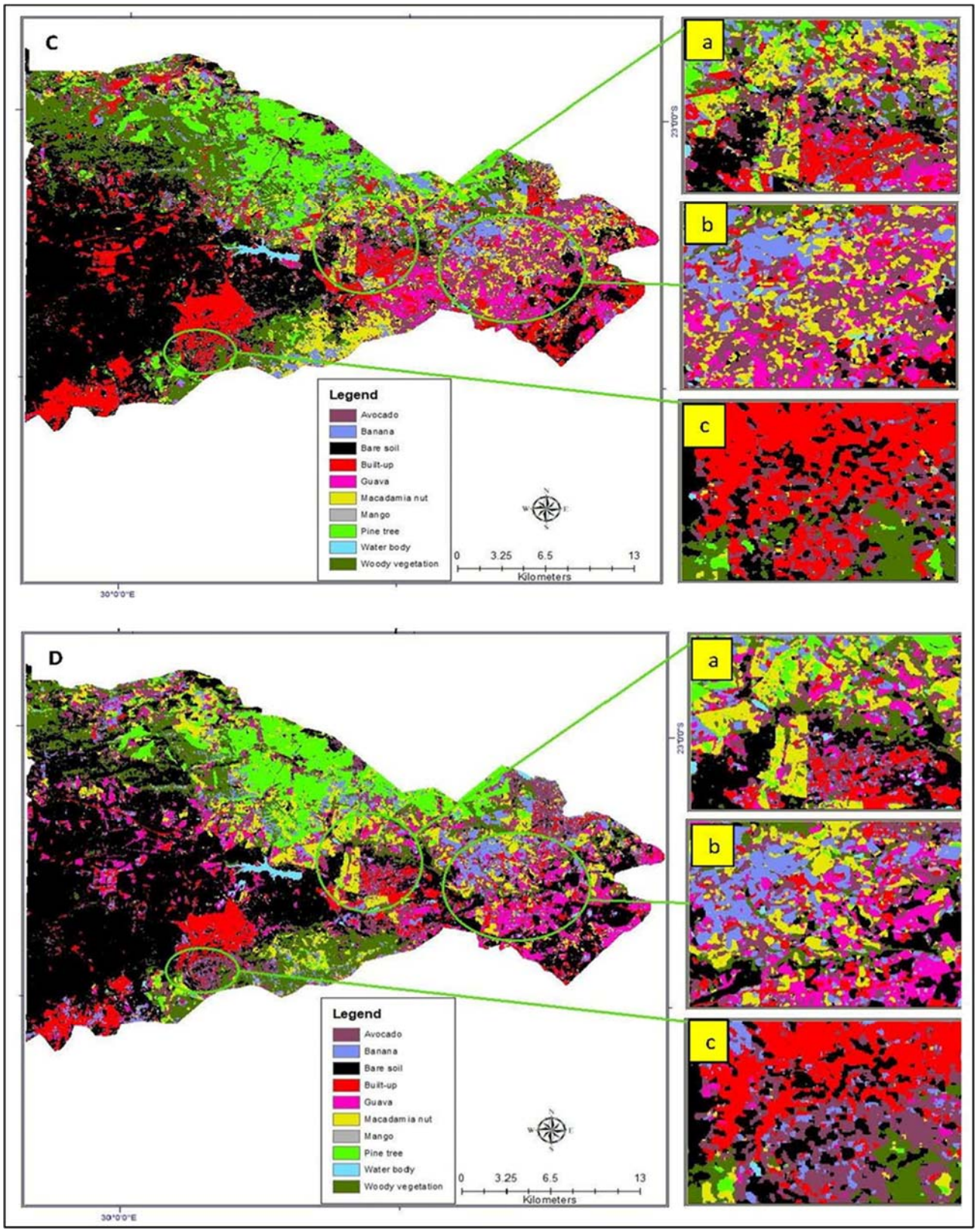

Figure 8: Classification maps of fruit tree crops with spatially explicit zoom-ins (a, b, and c), providing detailed spatial distributions from RF classifications in the research region for the best classification accuracy. They are based on four selected S2 monthly composite images captured in June (5A) and July 2019 (5B), and April (5C) and May 2020 (5D).

4. Discussion

The significance of this study was to identify the optimal temporal window in which crucial phenological stages can be used to effectively classify fruit tree crops in a highly fragmented heterogeneous horticultural landscape. The classification was perfoemd using Sentinel-2 (S2) dataset and a random forest (RF) classifier in a Google Earth Engine (GEE) environment. Furthermore, multi-temporal images allowed for the identification of an optimal phenology stage in which different fruit trees could be accurately differentiated from one another (Santos *et al.*, 2019).

The spectral reflectance of the crops was determined by a myriad of factors (e.g., fruit varieties, different management, and mixed cropping systems, etc.). Different crop varieties of the same family can furthermore have different growth stages (i.e., flowering, fruiting, or harvesting). As such, they exhibited different biochemical traits (Ren *et al.*, 2022). Figure 3 shows that within one standard deviation, all fruit tree classes showed varying but significant degrees of spectral overlap. The best four performing models (i.e., April, May, June and July models) revealed that beyond one standard deviation from the mean, only the green band (B3) separated macadamia from avocado, banana, guava, and mango. In May, again, the green band (B3) separated avocado from banana, guava, macadamia, and mango trees, while the shortwave-infrared (B11 and B12) bands differentiated guava trees from the other fruit tree classes. In the months of June and July also, beyond one standard deviation of uncertainty, the shortwave-infrared (B11 and B12) bands differentiated guava from avocado, banana, macadamia nut, and mango trees. However, an advantage of machine learning classifiers, such as RF, is that they are suited to extreme cases of binary classification, and as such, lead to highly accurate classifications (Kuter, 2021). The major objective in selecting variables is to choose and identify those of high importance, which makes the associated models simpler and faster to fit and to predict. Overall, the red band outperformed the other bands in the months of May, June, and July. The greatest contribution of the red band in differentiating between the respective fruit trees in the study area was in July (Figure 4). The best performing bands in April were the green (B3), shortwave-infared (B11), red-edge (B5), red (B4), and shortwave-infrared (B12) bands. The bands which performed dismally in the four best performing models were the near-infrared band in May, and the red-edge bands (i.e., B7 and B6) in the months of May and April, respectively. The near-infrared (B8) band performed well in July. Generally, the visible bands performed well in differentiating between the fruit tree crops in the study area.

The flowering of the fruit trees was detected mostly by the red (B4: 665 nm) and green (B3:560 nm) bands from the visible light spectrum, as these bands show correlations with the photosynthetic components (i.e., pigment, water, and chlorophyll) of the fruit trees (Pena *et al.*, 2017). Comparable with the findings of Peña and Brenning (2015), the green band was saturated at the end of the vegetative stage as a result of the high chlorophyll content, and contributed again in June and July, when the mango and macadamia nut crops started flowering, thus indicating that this band performs well at the green-up stage. Previous work has demonstrated that the near-infared bands are influential in differentiating between the crop types (Lakshmanan and Mathiyazhagan, 2019). In this study, the near-infared (B8A:865 nm) spectral band performed well and contributed substantially to the classification of crop types during the flowering stage. The highly predictive power of the near-infared (B8A:865 nm) band is attributed to its sensitivity to the vegetation metrics (i.e.,

chlorophyll, LAI, and nitrogen), which are in turn related to crop growth and productivity (Tu *et al.*, 2019). A reduced differential ability in the near-infrared region was apparent at the end of the fruiting stage and the start of the harvesting stage when crop classification favours clear differences in relation to the amount of foliage of the various crops (Pena *et al*., 2017). The observed multi-series signatures of the S2 bands concurred with those observed by Mercier *et al*. (2020). A peak variation in spectral signatures was recorded for the red-edge bands during the flowering and fruiting stages (Figure 8). Feng *et al.* (2019) and Figueroa-Figueroa *et al.* (2020) recently reported that the inclusion of shortwave-infrared and red-edge bands had a significant effect in distinguishing between the fruit tree crops. Their results concur with previous findings by Delloye *et al*. (2018). Comparable with the report by Luo *et al.* (2021), the red-edge (B5:705 nm) band proved to be a strong predictor during the senescent and fruiting stages because of its sensitivity to the chlorophyll levels. The high temporal resolution of S2, with its three additional spectral bands located in the red-edge position (REP), allowed for the retrieval of the vegetation parameters such as chlorophyll, leaf nitrogen content, and leaf area index (LAI) (Chabalala *et al*., 2020). The shortwave-infrared bands (B11:1610 nm, B12:2190 nm) could detect the variation in the water content and foliar chlorophyll of the fruit tree crops (Peña and Brenning, 2015). The results are supported by Ren *et al.* (2022), who highlighted the importance of shortwave-infrared bands in distinguishing between crop types.

The RF classification of S2 images (i.e., from June 2019 -May 2020), classified fruit trees with overall accuracies (OA) ranging from 67 - 84.80% and a kappa coefficient (κ) ranging from 67 - 83%. The winter images reported the highest accuracies in their classification results (i.e., OA greater than 80%). The results concur with previous crop-type mapping research findings by Blickensdörfer *et al.* (2022), who obtained the highest accuracies in their classification results of 80% using winter images. Research by Luo *et al*. (2021) achieved similar OA results of 89.75% when these researchers mapped crop types in China using S2 time series data at a regional level. The winter months (i.e., April - July), coincided with peak greenness (i.e., the fruiting period of most crops) (Luo *et al*., 2021). The user accuracy (UA) ranged from 60 to 100%, while the producer accuracy (PA) ranged from 58 to 100%. Owing to spectral similarities emanating from overlapping phenological stages, the UA and PA accuracies for banana, mango, and macadamia nut classes were low from January to March 2020, (Tu *et al.*, 2019; Kyere *et al.*, 2020). It is worth noting that these were crop growth periods during which Levubu experienced a high volume of rainfall (i.e., in 2020). The existence of double-row planting systems and a mixture of young ***versus*** mature macadamia and banana trees made it challenging to accurately detect such trees. Furthermore, since the banana crop is asynchronous, its growth stages often overlap with those of the avocado, mango, guava, and macadamia nut trees (Hebbar *et al.*, 2014; Gao *et al.*, 2020). The findings are consistent with observations by Hebbar *et al*. (2014), who reported poor classification accuracy in orchard plantations owing to mixed spectral reflectance emanating from the simultaneous presence of young and mature plantations. For example, the avocado and mango crops reported higher accuracy levels from their larger canopies and leaf structure. In contrast, the macadamia nut and banana classes produced lower classification accuracies for most months. This can be attributed to their canopy structures and the shape of their leaves that expose the soil background and result in mixed spectral signatures (Rajah *et al.*, 2017). Overall, the class accuracies of the fruit tree crop and the co-existing land cover types differed because of the differences in the spectral properties exhibited by the crops during their growth cycles (Ge *et al.*, 2016).

The results of this study proved that S2 images are sufficient for the accurate mapping of fruit trees in the fragmented horticultural landscapes of South Africa. The classification maps produced in this research could assist agronomists, horticulturists, and farm managers in devising precise management strategies to build sustainable horticultural food systems (Yi *et al*., 2020).

4.1. Limitations

Tracking crop growth by using multi-series data was limited by the prevailing cloud cover at the time of the research. The unavailability of quality images limited the accuracy during the summer months. The monitoring of the banana green-up and senescent stages was missed as a result of crop mismanagement and the presence of cloud in the S2 multi-temporal data from December to March. The problem was aggravated by the cloud and cloud shadow detection algorithms, that proved to be unreliable.

5. Conclusion

This research leveraged the power of the spatial and temporal resolution of S2 data analysed in a Google Earth Engine (GEE) environment and a RF classifier in mapping fruit trees. The results led to the conclusion that optimising the data acquisition period and the potential of temporal resolution in remote sensing offers considerable promise for accurately identifying fruit trees. The optimum period for establishing the type of fruit trees was during the early and middle growth stages (i.e., during the flowering and fruiting stages). This study has proved the Sentinel-2 (S2) sensor to be a useful tool for modelling and monitoring fruit trees at the landscape level. The results provide evidence-based information that could allow for efficient horticultural monitoring systems and sustainable agricultural management, particularly in countries or regions where specific crop databases are not available. The approach used in this study could be applied as a framework for areas with similar fruit tree types, phenologies, and landscape characteristics.

6. References

Arias, M; Campo-Bescós, MÁ; Álvarez-Mozos, J 2020, 'Crop classification based on temporal signatures of Sentinel-1 observations over Navarre province, Spain', *Remote Sensing*, vol.12, No. 2, pp. 1-29.

Asgarian, A; Soffianian, A; Pourmanafi, S 2016, 'Crop type mapping in a highly fragmented and heterogeneous agricultural landscape: A case of central Iran using multi-temporal Landsat 8 imagery', *Computer Electronics in Agriculture*, vol. 127, pp.531–540.

Bagheri, N. Application of aerial remote sensing technology for detection of fire blight-infected pear trees. *Computer and Electronics in Agriculture*. **2019**, 168, 105147. https://doi: 10.1016/j.compag.2019.105147.

Banko, G 1998, 'A Review of Assessing the Accuracy of Classifications of Remotely Sensed Data and of Methods, Including Remote Sensing Data in Forest Inventory' 1998, viewed on 16 November 2022, < Review of Assessing the Accuracy of Classifications of Remotely Sensed Data and of Methods, Including Remote Sensing Data in Forest Inventory - Search (bing.com) >.

Busetto, L; Zwart, SJ; Boschetti, M 2019, 'Analysing spatial–temporal changes in rice cultivation practices in the Senegal River Valley using MODIS time series and the PhenoRice algorithm', *International Journal of Applied Earth Observation and Geoinformation*, vol. 75, pp. 15–28.

Blickensdörfer, L; Schwieder, M; Pflugmacher, D; Nendel, C; Erasmi, S; Hostert, P 2022, 'Mapping of crop types and crop sequences with combined time series of Sentinel-1, Sentinel-2 and Landsat 8 data for Germany', Remote Sensing of the Environment, vol. 269, pp. 1-19.

Breiman, L. Random forests. Mach. Learn. 2001, 45, 5–32. Available online: https://link.springer.com/article/10.1023/A:1010933404324 (Accessed on 16 October 2022).

Central Statistical Agency. Agricultural Sample Survey 2010/2011, viewed on 18 November 2022, < https://www.scirp.org/(S(351jmbntvnsjt1aadkposzje))/reference/referencespapers.aspx?referenceid=2611368>

Congalton, R 1991, 'A review of assessing the accuracy of classifications of remotely sensed data', *Remote Sensing of Environment*, vol. 37, pp. 35–46.

Chabalala, Y; Adam, E; Oumar, Z; Ramoelo, A 2020, 'Exploiting the capabilities of Sentinel-2 and RapidEye for predicting grass nitrogen across different grass communities in a protected area', *Applied Geomatics*., vol.12, pp. 379–395.

Chabalala, Y; Adam, E, Ali, KA 2022, 'Machine Learning Classification of Fused Sentinel-1 and Sentinel-2 Image Data towards Mapping Fruit Plantations in Highly Heterogenous Landscapes' *Remote Sensing*, vol.14, pp.1-26.

Chabalala, Y.; Adam, E.; Ali, K.A. 2023, 'Exploring the Effect of Balanced and Imbalanced Multi-Class Distribution Data and Sampling Techniques on Fruit-Tree Crop Classification Using Different Machine Learning Classifiers. *Geomatics*, vol. 3, pp. 70-92.

Claverie, M.; Ju, J.; Masek, J.G.; Dungan, J.L.; Vermote, E.F.; Riger, J.C; Skakun S.V.; Justice, C. The Harmonized Landsat and Sentinel-2 surface reflectance data set. Remote Sensing of Environment. 2018, 219, 145–161. https://doi: 10.1016/j.rse.2018.09.002.

European Space Agency (ESA) 2023. on 01 September 2023 <https://sentinel.esa.int/web/sentinel/user-guides/sentinel-2-msi/processing-levels/level-2>.

Kolecka, N.; Ginzler, C.; Pazur, R.; Price, B.; Verburg, P. H. -scale mapping of grassland mowing frequency with Sentinel-2 time *Remote Sensing*. 10. https://doi: 10.3390/rs10081221.

Delloye, C; Weiss, M; Defourny, P 2018, 'Retrieval of the canopy chlorophyll content from Sentinel-2 spectral bands to estimate nitrogen uptake in intensive winter wheat cropping systems', *Remote Sensing of Environment*, vol. 216, pp. 245–261.

Feng, S; Zhao, J; Liu, T; Zhang, H; Zhang, Z; Guo, X 2019, 'Crop Type Identification and Mapping Using Machine-Learning Algorithms and Sentinel-2 Time Series Data', *IEEE Journal of Selected Topics in Applied Earth Observation and Remote Sensing,* vol.12, pp. 3295–3306.

Figueroa-Figueroa, DK; Ramírez-Dávila, JF; Antonio-Némiga, X; González Huerta, A 2020, 'Mapping of avocado in the south of the state of Mexico by digital image-processing -2', *Revista Mexicana de ciencias agrícolas*, vol.11, No. 4, pp. 865–879.

Fraser, A 2008, 'White farmers' dealings with land reform in Africa: Evidence from Northern Limpopo Province', *Tijdschrift voor Economische en Sociale Geografie* 99, pp. 24-36.

Gao, F; Anderson, M; Daughtry, C; Karnieli, A; Hively, D; Kustas, 2020, 'A within-season approach for detecting early growth stages in corn and soybean using high temporal and spatial resolution imagery', *Remote Sensing of Environment*, vol. 242, pp.111752.

Ge, Y; Bai, G; Stoerger, V; Schnable, JC 2016, 'Temporal dynamics of plant growth, water use, and leaf water content using automated high throughput RGB and hyperspectral imaging', Computer Electronics in Agriculture, vol. 127, pp. 625–63212.

Gutierrez-Coarite, R; Mollinedo, J; Cho, A; Wright, MG 2018, 'Canopy management of macadamia trees and understory plant diversification to reduce macadamia felted coccid (*Eriococcus ironsidei*) populations', *Crop Protection*, vol. 113, pp. 75–83.

Griffiths, P; Nendel, C; Hostert, P 2017, 'Intra-annual reflectance composites from Sentinel-2 and Landsat for national-scale crop and land cover mapping', *Remote Sensing of Environment*, vol. 220, pp. 135–151.

Hebbar, R; Ravishankar, HM; Trivedi, S; Subramoniam, SR; Raj, U; Dadhwal, VK 2014, 'Object-oriented classification of high resolution data for inventory of horticultural crops', *International Archives of the Photogrammetry, Remote Sensing and Spatial. Information Sciences. ISPRS Archives.*, vol. 40, 745–749.

Johansen, K; Duan, Q; Tu, YH; Searle, C; Wu, D; Phinn, S; Robson, A; McCabe, MF 2020, 'Mapping the condition of macadamia tree crops using multispectral UAV and WorldView-3 imagery', *ISPRS Journal of Photogrammetry and Remote Sens*ing, vol. 165, pp.28–40, 2020.

Jin, Z; Azzari, G; You, C; Di Tommaso, S; Aston, S; Burke, M, Lobell, DB 2019, 'Smallholder area and yield mapping at national scales with Google Earth Engine', *Remote Sensing of Environment*, vol. 228, pp.115–128.

Kumari, M; Pandey, V; Choudhary, KK; Murthy, CS 2021, 'Object-based machine learning approach for soybean mapping using temporal -1/-2 data', *Geocarto International*, vol. 37, pp. 6848-6866.

Kuter, S. 2021, 'Completing the machine learning saga in fractional snow cover estimation from MODIS Terra reflectance data: Random forests *versus* support vector regression', *Remote Sensing of Environment*, vol. 255, pp. 112294.

Kyere, I; Astor, T; Graß, R; Wachendorf, M 2020, 'Agricultural crop discrimination in a heterogeneous low-mountain range region based on multi-temporal and multi-sensor satellite data', *Computer and Electronics in Agriculture*, vol. 179, pp. 105864.

Rajah, P; Odindi, J; Abdel-Rahman, E; Mutanga, 2017, 'Determining the optimal phenological stage for predicting common dry bean (*Phaseolus vulgaris*) yield using field spectroscopy', *South African Journal of. Plant Soil*, vol. 34, pp. 379–388.

Lakshmanan, G; Mathiyazhagan, 2019, 'Machine-learning classifiers on Sentinel-2 satellite image for the classification of banana (*Musa Sp*.) plantations of Theni district, Tamil Nadu, India', *International Journal of Chemical Studies*, vol. 7, No. 5, pp.1419–1425.

Lamour, J; Lechaudel, ONM; Le Moguédec, G; Tisseyre, JTB 2019, 'Spatial analysis and mapping of banana crop properties : issues of the asynchronicity of the banana production and proposition of a statistical method to take it into account', *Precision Agriculture*, vol. 21, pp. 897-921.

Luo, C; Liu, HJ; Lu, LP; Liu, ZR; Kong, FC; Zhang, XL 2021, 'Monthly composites from Sentinel-1 and Sentinel-2 images for regional major crop mapping with Google Earth Engine', *Journal of Integrative Agriculture*, vol. 20, No.7, pp.1944–1957.

Mercier, A; Betdeer, J; Baudry. J; Le Roux, V; Spicher, F; Lacoux, J, Roger, D; Hubert-Moy, L 2020, 'Evaluation of Sentinel-1 & 2 time series for predicting wheat and rapeseed phenological stages', *ISPRS Journal of Photogrammetry and Remote Sensing*, vol. 163, pp. 231–256.

Maxwell, AE, Warner, TA, Fang, F 2018, ' Implementation of machine-learning classification in remote sensing: An applied review', International Journal of Remote Sensing, vol. 39, pp. 2784-2817.

Nabil, M; Farg, E; Arafat, SM; Aboelghar, M; Afify, NM; Elsharkawy, MM 2022, 'Tree-fruits crop type mapping from Sentinel-1 and Sentinel-2 data integration in Egypt's New Delta project', *Remote Sensing Applications: Society and Environment*, vol. 27, pp. 100776.

Ni, R; Tian. J; Li, X; Yin, D; Li, J; Gong, H; Zhang, J; Zhu, L; Wu, D 2021, 'An enhanced pixel-based phenological feature for accurate paddy rice mapping with Sentinel-2 imagery in Google Earth Engine', *ISPRS Journal of Photogrammetry and Remote Sensing*, vol. 178, pp. 282–296.

Olofsson, P; Foody, GM; Herold, M; Stehman, SV; Woodcock, CE; Wulder, MA 2014, 'Good practices for estimating area and assessing accuracy of land change', *Remote Sensing of Environment*, vol.148, pp. 42–57.

Paris, C; Weikmann, G; Bruzzone, L 2020. 'Monitoring of agricultural areas by using Sentinel 2 image time series and deep learning techniques', vol. 115, No. 2, pp.136-153.

Peña, MA; Brenning, A 2015, 'Assessing fruit-tree crop classification from Landsat-8 time series for the Maipo Valley, Chile', *Remote Sensing of Enviroment,* vol. 171, pp. 234–244.

Peña-barragán, JM; Ngugi, MK; Plant, RE; Six, J 2011, 'Object-based crop identification using multiple vegetation indices, textural features and crop phenology', *Remote Sensing of Environment*, vol.115, pp.1301–1316.

Potgieter, AB; Zhao, Y; Zarco-Tejada, PJ; Chen, K; Zhang, Y; Porker, K; Biddulph, B; Dang, YP; Neale,T; Roosta, F; Chapman, S 2021, 'Evolution and application of digital technologies to predict crop type and crop phenology in agriculture', *In Silico Plants*, vol 3, no. l, pp.1–23.

Remelgado, R.; Zaitov, S.; Kenjabaev, S 2020, 'A crop type dataset for consistent land cover classification in Central Asia', *Scientific Data*, vol. 7, pp. 1–6.

Ren, T; Xu, H; Cai, X; Yu, S; Qi, J 2022, 'Smallholder Crop Type Mapping and Rotation Monitoring in Mountainous Areas with Sentinel-1/2 Imagery', *Remote Sensing*, vol. 14, No. 22, pp. 566.

Saini, R & Ghosh, SK Crop Classification on Single Date Sentinel-2 Imagery Using Random Forest and Support Vector Machine. *ISPRS - International Archives of the Photogrammetry, Remote Sensing and Spatial Information Sciences*. 2018, 5, 683–688. https://doi: 10.5194/isprs-archives-xlii-5-683-2018.

Santos, CLM, de O; Lamparelli, RAC; Figueiredo, GKDA; Dupuy, S; Bouty, J; Luciano, AC, dos S 2019, 'Classification of crops, pastures, and tree plantations along the season with multi-sensor image time series in a subtropical agricultural region', *Remote Sensing*, vol. 11, pp. 1–27.

Singh, V; Patel, AN; Dalwadi, A; Kathota, J; Suthar, J 2017, 'Horticultural Fruit Crop Plantations Mapping using Geo-informatics Technology in Gujarat State, India', *International Journal of Advanced Remote Sensing and GIS*, vol. 6, pp. 2033–2049.

Sinha, P; Robson, A; Schneider, D; Kiic, T; Mugera, HK; Ilukor, J; Tindamanyire, JM 2020, 'The potential of *in-situ* hyperspectral remote sensing for differentiating 12 banana genotypes grown in Uganda', *ISPRS Journal of Photogrammetry and Remote Sensing*, vol. 167, pp. 85–103.

Shelestov, A; Lavreniuk, M; Kussul, N; Novikov, A; Skakun, S 2017, 'Exploring Google Earth Engine platform for big data processing: Classification of multi-temporal satellite imagery for crop mapping', *Frontiers of Earth Science,* vol. 5, pp.1–10.

Tu, Y. H.; Johansen, K.; Phinn, S.; Robson, A 2019, 'Measuring canopy structure and condition using multispectral UAS imagery in a horticultural environment', *Remote Sensing, vol.* 11, 15–17. https://doi: 10.3390/rs11030269.

Tatsumi, K; Yamashiki, Y; Canales Torres, MA; Taipe, CLR, ' Crop classification of upland fields using Random Forest of time-series Landsat 7 ETM+ data', *Computer and Electronics in Agriculture*, vol. 115, pp.171–179.

Usha, K, Singh, B 2013, 'Potential applications of remote sensing in horticulture: A review', *Scientia Horticulture***,** vol. 153, pp. 71–83.

Valero, S; Arnaud, L; Planells, M; Ceschia, E 2011, 'Synergy of Sentinel-1 and Sentinel-2 imagery for early seasonal agricultural crop mapping', *Remote Sensing*, vol. 13, pp. 1–32.

Veloso, A; Mermoz, S; Bouvet, A; Le Toan, T; Planells, M; Deroux, JF, Ceschia, E 2017, 'Understanding the temporal behavior of crops using Sentinel-1 and Sentinel-2-like data for agricultural applications', *Remote Sensing of Environment*, vol. 199, pp. 415–426.

Vuolo, F; Neuwirth, M; Immitzer, M; Atzberger, C; Ng, W 2018, 'How much does multi-temporal Sentinel-2 data improve crop-type classification?', *International Journal of Applied Earth Observation &Geoinformation*, vol.72, pp.122–130.

Waldner, F; Bellemans, N; Hichman, Z; Newby, T; de Abelleyra, D; Veron, SR, Bartalev, S; Lavreniuk, M; Kussul, N; Maire, GL; Simoes, M; Skakun, S; Defoury, P 2019, 'Roadside collection of training data for cropland mapping is viable when environmental and management gradients are surveyed', *International. Journal of Applied Earth Observation & Geoinformation*, vol. 80, pp. 82–93.

Yang, H; Pan, B; Li, N; Wang, W; Zhang, J; Zhang, X 2021, 'A systematic method for spatio-temporal phenology estimation of paddy rice using time series Sentinel-1 images', *Remote Sensing of Environment*, vol. 259, pp. 112394.

Yi, Z; Jia, L; Chen, Q 2020, 'Crop classification using multi-temporal Sentinel-2 data in the Shiyang river basin of China', *Remote Sensing*, vol.12, pp. 1–21.

You, N; Dong, J 2019, 'Examining earliest identifiable timing of crops using all available Sentinel 1/2 imagery and Google Earth Engine', *ISPRS Journal of Photogrammatic Remote Sensing*, vol.161, pp.109–123.

Zurita-Milla, R; Izquierdo-Verdiguier, E; De By, RA 2017, 'Identifying crops in smallholder farms using time series of WorldView-2 images', *9th International Workshop Analysis of Multitemporal Remote Sensing Images,* pp. 21–23.

Zhang 'Object-based crop classification using multi-temporal SPOT-5 imagery and textural features with a Random Forest classifier'. *Geocarto International*. 2018, 33, 1017–1035.

Zhang, P; Hu, S; Li, W; Zhang, C 2020, 'Parcel-level mapping of crops in a smallholder agricultural area: the case of Central China using single-temporal VHSR imagery', *Computer and Electronics in Agriculture*, vol.175, pp. 105581.

Zhi, F.; Dong, Z.; Guga, S.; Bao, Y.; Han, A.; Zhang, J.; Bao, Y. 2022, 'Rapid and Automated Mapping of Crop Type in Jilin Province Using Historical Crop Labels and the Google Earth Engine', *Remote Sensing*, vol.14, pp. 4028.